JℱM PAPERS

Spatial growth rates of young wind waves under steady wind forcing

Krishanu Kumar[1] and Lev Shemer[1],†

[1]School of Mechanical Engineering, Tel-Aviv University, Tel-Aviv 69978, Israel

The growth with fetch of young wind waves under steady wind forcing that is commonly attributed to shear flow instability results in a spatially inhomogeneous wave field with a spectrum evolving along the tank. The present laboratory study accounts for multiple co-existing statistically stationary random frequency harmonics. Single-point synchronous measurements of the instantaneous surface elevation and of its along-wind slope component are performed by optical methods at numerous locations. Assuming exponential spatial growth, the phase shift between the surface elevation and surface slope at each frequency is related to the spatial growth rate of each harmonic. The validity of the assumption that the wave energy varies exponentially with fetch is examined in a separate set of experiments; the instantaneous surface elevation at various wind-forcing conditions is measured at multiple locations along the tank. The spatial variation of the energy of individual frequency harmonics is determined. It is found that, below the local peak frequency, the energy of each harmonic grows exponentially, while the evolution of waves at frequencies approaching and exceeding the local peak is strongly affected by sheltering by the dominant wave, as well as by nonlinear bound waves. The outcomes of two independent methods of determination of spatial growth rates at a range of young wave frequencies are compared. The accumulated data also enable quantitative analysis of the sheltering phenomenon. The essential difference between the spatial and the temporal wind-wave evolution cases is discussed.

Key words: wind-wave interactions, surface gravity waves, shear-flow instability

1. Introduction

Starting from Jeffreys ([1925](#)), Phillips ([1957](#)) and Miles ([1957](#)), significant efforts were invested in attempts to understand the mechanisms governing energy and momentum

† Email address for correspondence: shemerl@tauex.tau.ac.il

984 A22-1

exchange between air and water. Theoretical studies were accompanied by experiments in laboratory and field settings. Nevertheless, the details on the initial inception and of the subsequent growth of wind-generated waves are still not sufficiently well understood. The approach adopted in Miles (1957) and numerous subsequent studies by him and other authors considers temporal growth of the amplitude of a harmonic of a gravity wave with a fixed wavenumber k under the action of an impulsively applied wind above an initially quiescent water surface. The wave growth in those theories is attributed to the shear flow instability. The linear Miles model thus predicts that each initially infinitesimal unstable harmonic grows exponentially in time; the growth rate depends on the vertical mean velocity profile in airflow and on the wavenumber k. An alternative theory by Phillips (1957) relates the growth of random waves to resonant and non-resonant turbulent pressure fluctuations in the wind over the water surface. Unlike the unidirectional and deterministic shear flow instability theory, the Phillips model emphasized the three-dimensional and random nature of the wind-wave field.

The theories of Miles and Phillips deal mainly with the initial stages of evolution in time of wind waves excited by an impulsively applied horizontally homogeneous wind, while Jeffreys (1925) considered the evolution of already existing wind waves and explained the wave growth by a sheltering mechanism that results in an asymmetric pressure distribution over the wave surface by fully separated airflow. This approach was further developed by Belcher & Hunt (1993) based on non-separated airflow over waves.

The refined version of the inviscid shear flow instability model by Miles (1960) estimates the growth of energy E of wind waves with initially small amplitude as

$$\frac{1}{E}\frac{\partial E}{\partial t} = \beta \frac{\rho_a}{\rho_w} \left(\frac{u_*}{c}\right)^2 \omega = \gamma, \tag{1.1}$$

where γ is the temporal growth rate, β is the dimensionless growth coefficient determined for each frequency $\omega(k)$ from the solution of the governing Rayleigh equation, u_* and c are the friction and the phase velocities, ω is the radian wave frequency and ρ_a, ρ_w are the air and water densities. Plant (1982) compiled an extensive set of data accumulated in field and laboratory experiments. He adopted the Miles equation (1.1) and suggested the value of the temporal growth coefficient $\beta = 35 \pm 16$ as the best fit to the experimental results. This relation is still widely used for estimating the temporal energy growth rate γ.

Experiments carried out by Synder *et al.* (1981) in an attempt to examine the Phillips theory of wave generation due to turbulent pressure fluctuations demonstrated that this mechanism is insufficient to account for the observed growth rates. Contrary to that, numerous experiments indicated that there is at least qualitative agreement between experimental results and the Miles (1957) model (Shemdin & Hsu 1967; Bole & Hsu 1969; Larson & Wright 1975), resulting in the wide acceptance of the shear flow instability theory as the primary model of wave generation and growth. However, this inviscid theory disregards wind-induced shear flow in water that affects the dispersion relation of short gravity–capillary waves. The theoretical predictions based on Miles (1957) therefore underestimate the growth rate measured by Larson & Wright (1975). Valenzuela (1976) extended Miles' inviscid theory to account for viscosity and derived a set of coupled Orr–Sommerfeld (OS) equations in air and water to study viscous shear flow instability. His model computations demonstrated better agreement with the results of Larson & Wright (1975). In a subsequent more detailed study, Kawai (1976) measured the growth of initial wavelets under impulsive wind forcing and found a limited quantitative agreement with Miles (1960); following Valenzuela (1976), he also applied the coupled OS theory to explain the initial wavelets' inception and their growth in time.

Experimental conditions where waves are excited by an impulsively applied wind forcing over an initially quiescent water surface are often referred to as a 'duration-limited case'. The temporal variation of wind waves in this case is thus assumed to be independent of fetch x. However, laboratory experiments performed under such excitation conditions by Mitsuyasu & Rikiishi (1978) and Zavadsky & Shemer (2017*b*) demonstrated that, for each fetch x_0, the wave field can be seen as spatially homogeneous at all fetches $x > x_0$ only for a certain duration t_0 that increases with x_0. At the instant $t_0(x_0)$, a transient process is initiated in which the wave energy at x_0 starts to increase faster than that at longer fetches. This transient process eventually leads at each x_0 to a final quasi-steady state, which is statistically stationary but spatially inhomogeneous for $x < x_0$. Zavadsky & Shemer (2017*b*) and Geva & Shemer (2022*a*) related the time elapsed from the wind initiation to attaining the steady state t_0 at each fetch x_0 to the group velocity c_g corresponding to the local peak frequency f_p, $t_0 = x/c_g(f_p)$.

Larson & Wright (1975) were the first to apply a single wavenumber-sensitive radar-based technique that is capable of measuring the temporal growth of the energy of wind waves with the wavenumber that is in Bragg resonance with the radar wavelength. Larson & Wright (1975) and Plant & Wright (1977) used this method to directly measure the initial temporal growth of wind waves under impulsive wind forcing and compared them with Miles' predictions. Plant & Wright (1977) performed those experiments at multiple locations and therefore were also able to estimate the spatial growth rate of a single wave harmonic under steady wind forcing. Later, attempts to apply the radar technique in field experiments by Stewart & Teague (1980), however, lacked sufficient accuracy to extract reliable data comparable to theoretical predictions due to various parameters that affect the wave field such as changes in the direction and magnitude of the wind, effects of bathymetry, currents, etc. More recently, the results of measurements of turbulent velocity fluctuations and surface elevation carried out in open ocean by Hristov, Miller & Friehe (2003) were shown to be consistent with the presence of critical layer mechanism for the wind-wave coupling.

The vast majority of laboratory experiments are performed under steady wind forcing; the wave field is then statistically stationary in time and evolves in space, the so-called 'fetch-limited case'. In some studies, the rate of energy growth with fetch of a mechanically generated deterministic wave with an initially small steepness is determined by exponential fitting (see Bole & Hsu (1969); Mitsuyasu & Honda (1982); Peirson & Garcia (2008) and Zhang *et al.* (2023) and references therein). The obtained values of the spatial growth rates α are then translated into temporal growth rates γ using the wave group velocity, $\gamma = c_g \alpha$ (Gaster 1962; Zeisel, Stiassnie & Agnon 2008). The presence of a dominant mechanically generated wave, however, may strongly affect the spatial evolution of the whole wind-wave spectrum (Shemer & Singh 2021).

Alternatively, attempts were made to evaluate the growth rate of wind waves at the dominant frequency in a statistically stationary wind-wave field by measuring the variation of the instantaneous surface elevation $\eta(t)$ and of the normal and/or shear stresses at a single point. In some of those studies, it is assumed that the wave energy at, or in the vicinity, of the local spectral peak represents the whole energy of the wave field. Such experiments were carried out in the laboratory (Shemdin & Hsu 1967; Liberzon & Shemer 2011; Grare *et al.* 2013; Buckley, Veron & Yousefi 2020) as well as in the field (Synder *et al.* 1981; Donelan *et al.* 2006). The measurements close to random air–water interfaces are notoriously difficult. The resulting estimates necessarily invoke some physical assumptions; the effect of viscous shear stress on the growth of waves is often neglected, on other occasions the normal stresses are only evaluated indirectly.

Obtaining the required phase information is complicated; extrapolation of quantities measured at some elevation above the interface to the instantaneous water surface that is often required is necessarily inaccurate and results in a large scatter of results.

2. Motivation

In nature, wind-generated wave fields are neither stationary nor homogeneous. The shear flow instability theory is based on the Fourier decomposition of the wave field; it is thus applicable either under the assumption of spatially homogeneous conditions, where the Fourier components are defined by the wave vectors $\boldsymbol{k}$ (or the wavenumbers k in the unidirectional case), or by their frequencies $\omega = 2\pi f$ under the assumption that wave parameters at each location are statistically stationary and do not vary in time.

Zeisel *et al.* (2008) applied coupled OS equations in air and water to study separately unidirectional linear temporal and spatial instabilities in the duration-limited and the fetch-limited cases, respectively. They demonstrated that the corresponding temporal γ and spatial α exponential growth rates for waves that satisfy the dispersion relation $\omega = \omega(k)$ are indeed related by the group velocity $c_g = \mathrm{d}\omega/\mathrm{d}k$. It should be emphasized, however, that temporal and spatial analyses deal with different physical realities. The temporal OS approach predicts the exponential growth in time with the rate $\gamma(k)$ of a spatially uniform harmonic with a fixed wavenumber. Contrary to that, the spatial analysis yields the exponential growth with x of a given frequency harmonic $\alpha(f)$, while its energy at a fixed location remains constant in time.

Recently, sophisticated numerical methods were applied to study the growth of wind waves under impulsive wind forcing over a quiescent water surface, or under steady forcing over young wind waves (see Yang & Shen (2010); Li & Shen (2022) Wu, Popinet & Deike (2022) and references therein). Those computations for the duration-limited conditions are usually carried out in the wave vector space, thus implying spatial homogeneity. As emphasized above, the computational results are therefore applicable only to the short initial evolution stages during which the wave field homogeneity is maintained. The fetch-limited stationary wind waves evolving under steady forcing are in this sense simpler, allowing their description in the frequency Fourier space. Note that the spatial version of the linear equation (1.1) predicts exponential with fetch growth of wave energy $E(x)$. However, the results of numerous field and laboratory experiments summarized in Zakharov *et al.* (2015) and in Shemer (2019) show that the spatial variation of the characteristic wave field parameters, such as the total wave energy $E(x)$ and the dominant (or peak) frequency $f_p(x)$, are well described by power laws. The exponent corresponding to the measured growth of $E(x)$ is close to unity, so that the energy increases nearly linearly rather than exponentially with fetch.

Shemer, Singh & Chernyshova (2020) attempted to reconcile this controversy in their phenomenological model of evolving fetch-limited wind waves by considering each harmonic in the discrete frequency spectrum. The measured spectrum at a short fetch served in their simulations as the initial condition. For each discrete spectral component f_i, they modelled wind input using the spatial version of (1.1) for the energy of each frequency harmonic $E_i = E(f_i)$

$$\frac{1}{E_i} \frac{\mathrm{d}E_i}{\mathrm{d}x} = \alpha_i, \tag{2.1}$$

where $c_{g,i} = c_g(f_i)$ and $\alpha_i = \gamma(f_i)/c_{g,i}$ is the spatial growth rate coefficient. The wind input was assumed to act only in the vicinity of the local dominant frequency. Viscous dissipation with the effective kinematic viscosity ν_{eff} was accounted for by adding the term

$-4\nu_{eff}k^2$ to the right-hand side of (2.1). This modification, as well as the dependence of the group velocity on frequency, allowed them to obtain in their simulation a certain growth of the wave energy with fetch, as well as a limited frequency downshifting. However, the linear model was incapable of predicting the rates of variation of $E(x)$ and $f_p(x)$ observed in experiments. Inspired by Zakharov *et al.* (2015), who attributed the linear wave energy growth of the duration-limited wind waves mainly to nonlinear wave–wave interactions, they introduced additional nonlinear terms in the evolution equation (2.1). Monte Carlo numerical simulations were then carried out using the resulting unidirectional spatial Zakharov equation. In each realization of the initial mean spectrum, phases and amplitudes of all harmonics were randomized. Adjustment of two empirical coefficients, β and ν_{eff} in this phenomenological model, allowed for the qualitative prediction of the spatial evolution of the energy and the dominant frequency of young gravity–capillary wind waves observed in the laboratory facility.

A novel approach to studying the evolution in space and time of waves excited by impulsive wind forcing was applied by Geva & Shemer (2022*a*). They analysed the evolving wave field as a stochastic ensemble of multiple wavenumber harmonics, all having identical initial amplitudes and probabilities. The model is quasi-linear and does not account for nonlinear wave–wave interactions. The dispersion relation and the temporal growth rates of each harmonic were computed for the adopted mean velocity profiles using the coupled OS equations in air and water. Although the OS equations are deterministic, the surface elevation at each fetch and instant was evaluated as an expected value of the stochastic ensemble of independent events. The wave growth of each harmonic was attributed solely to viscous shear flow instability as predicted by the OS equations, nonlinear effects were accounted for by limiting the maximum possible wave steepness; a limit was imposed on the growth duration of each harmonic at each fetch due to its final group velocity. Geva & Shemer (2022*a*) were able to describe in detail the various stages of wave evolution under impulsive wind forcing as recorded in experiments by Zavadsky & Shemer (2017*b*).

This achievement highlighted the importance of two factors in any attempt to present a model of wind waves that can be verified by experiments. First, the random character of wind waves needs to be accounted for. Second, detailed information on the evolution of various harmonics in the spectrum is needed. The present study of fetch-limited wind waves is designed to provide the necessary insight derived from detailed measurements under controlled conditions in view of those guidelines.

3. Experimental set-up and procedure

The experiments were carried out in a wind-wave facility with a 5 m $\times$ 0.4 m $\times$ 0.5 m test section made of glass and filled with distilled water up to 0.18 m depth. Airflow in a closed loop wind tunnel atop the test section is generated by a computer-controlled blower. The wind tunnel has large settling chambers at the entrance and the exit of the test section; the converging nozzle at the entrance ensures uniform flow. A sloping beach is installed at the end of the test section to reduce wave reflection. The instantaneous surface elevation $\eta(t)$ is measured simultaneously by a rake of 5 capacitance-type wave gauges made up of 0.5 mm diameter tantalum wires that are supported by a horizontal bar with a spacing of 10 cm between the adjacent sensors; the bar is fixed on a moving vertical stage connected to a carriage that can be placed at any desired location along the tank. Measurements were performed at carriage positions corresponding to the first probe in the rake located at distances $x = 100, 150, 200, 250$ and 300 cm from the inlet, thus

Blower setting (%)	U (ms^{-1})	u_* (ms^{-1})	U_{10} (ms^{-1})
25	5.54	0.37	9.36
30	6.83	0.44	11.77
35	8.10	0.52	14.05
40	9.35	0.57	16.43

Table 1. Representative maximum wind velocity, U, friction velocity, u_*, and wind velocity estimated at the elevation above the water surface at $z = 10$ m, U_{10}.

covering 25 fetches along the test section. A Pitot tube placed 10 cm above the mean water surface was used to monitor the air velocity. Data were recorded at four blower settings that determined the wind velocity in the test section. The representative wind velocities U, the corresponding friction velocities u_* and the wind velocities extrapolated to the elevation $z = 10$ m above the mean water surface U_{10} are given in table 1, which is based on the detailed measurements of logarithmic velocity profiles in the airflow above the wind waves (Zavadsky & Shemer 2012; Kumar, Geva & Shemer 2023). For each blower setting and each carriage position, the outputs of all sensors were sampled continuously for 900 s at the rate of 200 Hz channel^{-1}. More details on the facility and data acquisition procedure are given in Liberzon & Shemer (2011).

In a separate series of experiments, the surface elevation $\eta(t)$ and its orthogonal slope components in the wind direction $\eta_x = \partial\eta/\partial x(t)$, and in the cross-wind direction $\eta_y = \partial\eta/\partial y(t)$, were also measured synchronously using an optical wave gauge installed on a frame detached from the main facility that can be moved along the test section. The sensor consists of a laser slope gauge (LSG) for measurements of the instantaneous surface slope components $\eta_x(t)$, $\eta_y(t)$, and a high-speed camera that records the instantaneous vertical location of the laser beam tip that is visible in water but not in air, which is then translated into surface elevation $\eta(t)$. The camera is synchronized with the LSG using LabView software. For a detailed description of the optical sensor and its operational principles see Kumar, Singh & Shemer (2022), Zavadsky, Benetazzo & Shemer (2017) and Zavadsky & Shemer (2017a, 2018). Measurements of the surface elevation $\eta(t)$ and of the slope components $\eta_x(t)$ and $\eta_y(t)$ were performed for 900 s at the rate of 150 Hz channel^{-1} at 6 fetches, $x = 120, 180, 211, 245, 296$ and 335 cm at wind-forcing conditions identical to those in experiments with conventional wave gauges.

4. Frequency-dependent spatial inhomogeneity and the spatial growth rate

As emphasized above, the complexity of the wave field excited by time-dependent forcing that evolves both in space and time makes it difficult to identify the variation of individual harmonics in experiments. The radar technique, which is sensitive to a single wave vector component, is probably the only one available to study directly the wave's temporal growth. Using this technique, Larson & Wright (1975) and Plant & Wright (1977) demonstrated that, under impulsive excitation by wind, the wave energy of each harmonic at a given fetch grows exponentially in time until saturation is attained. Laboratory measurements by radar-based technique, however, are limited to short waves with fixed lengths in the gravity and gravity–capillary range. Experiments under steady wind forcing where the wave field is stationary are free of this limitation and enable us to obtain statistically reliable frequency spectra of the surface elevation. The spatial inhomogeneity of the wave field can be assessed by analysing the spatial variation of the
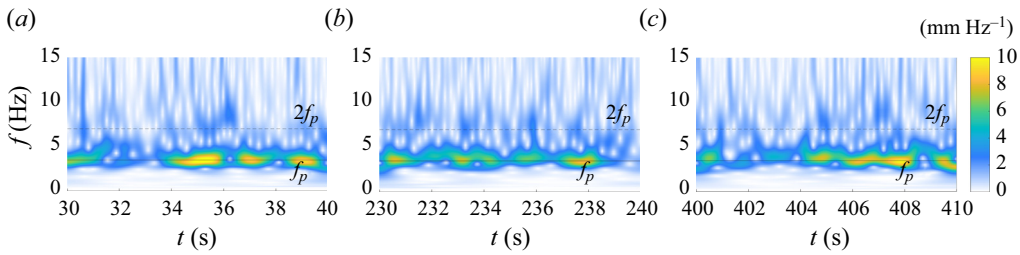
Figure 1. Wavelet spectrogram of surface elevation $S_\eta(f, t)$ as a function of frequency and various time instances; $x = 335$ cm and $U = 8.10$ m s^{-1}.

energy of individual harmonics. Moreover, these measurements allow us to account for the limited spatial coherence of wind waves (Shemer 2019; Shemer & Singh 2021).

The stochastic nature of the wave field generated by a steady forcing is clearly visible in examples of 10 s long instantaneous wavelet spectrograms of surface elevation $S_\eta(f, t)$ at arbitrarily selected initial instants presented in figure 1. The wavelet analysis follows that presented in Zavadsky & Shemer (2017b) and is based on a continuous Morlet wavelet transform that decomposes the time-varying function into wavelets as a function of frequency at each instant. A vertical section of the 'spectrum', or 'map', in figure 1 at any time t thus gives the instantaneous wavelet 'amplitudes' as a function of frequency, while a horizontal section at a frequency f yields the temporal variation of the wavelet 'amplitude' at this particular frequency. The spectrograms clearly show the coexistence of waves with multiple instantaneous 'frequencies' at any given instant; their instantaneous 'amplitudes' vary notably with time. Nevertheless, in most instances t in all panels of figure 1, there is a prominent peak at approximately 3.5 Hz, in agreement with the peak spectral frequency f_p obtained at those experimental conditions using temporal Fourier analysis.

4.1. *Spatial evolution of the energy of frequency harmonics along the tank*

To study the spatial variation of individual discrete harmonics in the wind-wave field, the energy spectra of the temporal variation of the surface elevation measured in the present experiments are used first. The statistical reliability of the wave energy estimates at multiple harmonics is attained by averaging the 180 power spectra computed for each 10 s long segment with 50 % overlap, taken from the 900 s long records of outputs of each wave gauge. In figure 2(a), the resulting averaged power spectra are plotted for $U = 6.83$ m s^{-1} at several fetches (the frequency resolution $\Delta f = 0.1$ Hz). This panel shows that the peak frequency f_p decreases and the wave energy at the peak increases with fetch. The dependence on fetch of the total wave energy $E_t(x) = \overline{\eta^2}(x)$ and of the peak frequency $f_p(x)$ are plotted in figure 2(b,c). The present results are consistent with the fetch relation suggested by Mitsuyasu (1970) and agree with the previous results obtained in our facility (Zavadsky, Liberzon & Shemer 2013; Shemer 2019).

A closer look at the spectra in figure 2(a) prompts examination of the characteristic wave energy variation along the tank separately for three ranges: at frequencies that at all fetches are well below the local peak frequency $f_p(x)$ (denoted by the black arrow in figure 2a); at frequencies that are below the local $f_p(x)$ at shorter fetches but exceed $f_p(x)$ at larger values of x (red arrow), and at higher frequencies that exceed $f_p(x)$ practically along the whole test section (blue arrow). The variation of the energy of the marked harmonics with fetch is plotted in figure 3(a) for all 25 fetches. This panel shows that, for the low frequency
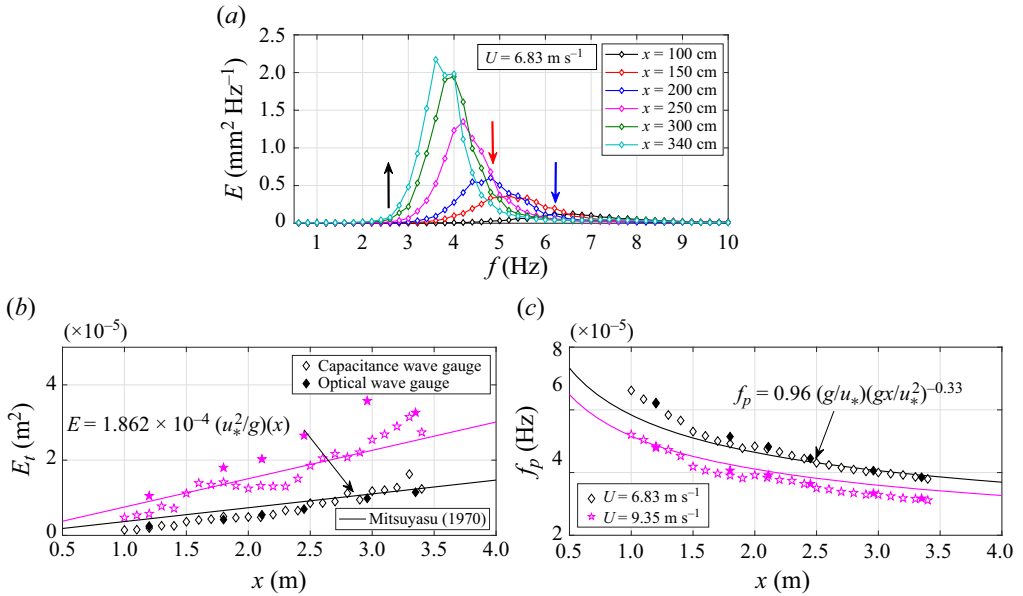
Figure 2. Energy spectra of wind waves at several fetches (*a*). Variation with fetch at two wind velocities *U* of (*b*) total wave energy $E_t(x)$; (*c*) the peak frequency $f_p(x)$.
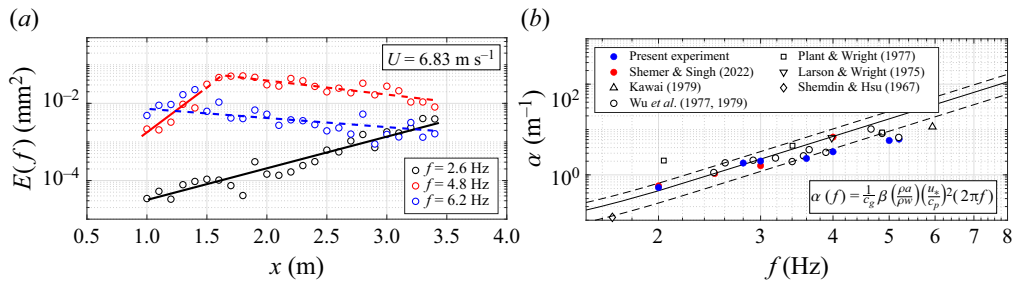

Figure 3. Variation of wave energy of (*a*) harmonics along the fetch, solid lines denote exponential growth, (*b*) spatial energy growth rate, $\alpha(f)$ as a function of f at $U = 6.83$ m s^{-1} and $u_* = 0.44$ m s^{-1}; solid and dashed lines: $\beta = 35 \pm 16$.

$f = 2.6$ Hz $< f_p(x)$ for all values of x, the wave amplitude grows approximately exponentially everywhere in the test section. For $f = 4.8$ Hz, which is below the peak frequency only for $x < 1.6$ m, the wave energy exhibits exponential growth up to $x \approx 1.6$ m and then tends to decrease; the energy decay with x can be approximated reasonably well by an exponent. The energy of the $f = 6.3$ Hz harmonic, which is mostly above the local f_p already at $x > 1.2$ m, decreases in figure 3(*a*) along the test section; the slope of the exponential decay is comparable to that of the 4.8 Hz harmonic.

The variation of the energy of each harmonic with fetch, as presented in figure 3(*a*), was examined for all wind velocities U employed in the present experiments, see table 1. For each frequency, an exponential growth fit limited to sufficiently short fetches allowed direct evaluation of the spatial energy growth rates $\alpha(f)$ that are plotted in figure 3(*b*). Plant (1982) complied the temporal energy growth rates $\gamma(f)$ accumulated in various field and laboratory experiments at $u_* \approx 0.44$ m s^{-1}; he used the group velocity $c_g(f) = \partial\omega/\partial k$ based on a linear dispersion relation for deep gravity–capillary waves,
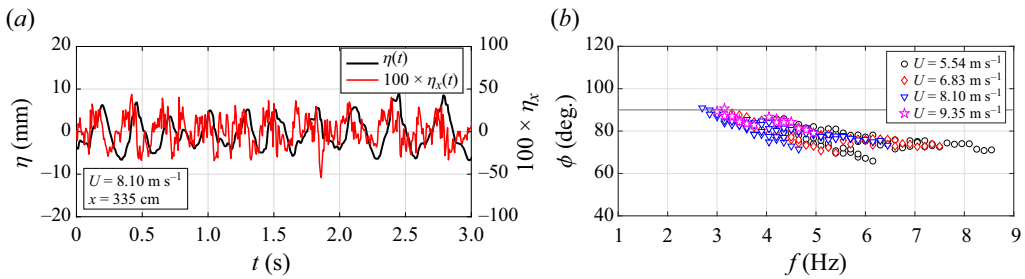
984 A22-8

(a)

(b)

Figure 4. (a) Short representative segment of time series at $x = 335$ cm and $U = 8.10$ m s^{-1}. (b) Phase difference between surface elevation η and along-wind slope η_x, $\phi(f)$.

$\omega^2 = gk(1 + \sigma k^2/g)$, to relate the spatial $\alpha(f)$ and the temporal $\gamma(f)$ growth rates. Figure 3(b) demonstrates that the growth rates $\alpha(f)$ based on the direct measurements of the energy growth of each harmonic agree well with the results obtained by different methods in various field and laboratory experiments. This also demonstrates the existence of exponential growth of wing-generated waves at frequencies $f < f_p(x)$ and provides additional support to the validity of the linear shear flow instability theory in describing the initial stages of wind-wave excitation.

4.2. *Spatial growth rate evaluation based on phase shift between the surface elevation and the along-wind surface slope*

An alternative approach to the evaluation of the spatial growth rate of wind waves is now suggested that is based on synchronous single-point measurements of $\eta(t)$ and $\eta_x(t)$. A segment of such a record presented in figure 4(a) for $U = 8.10$ m s^{-1} and $x = 335$ cm illustrates that both records have roughly the same dominant frequency of approximately $3 \sim 3.5$ Hz but exhibit a visible phase shift. The phase shift between time-dependent functions $F(t)$ and $G(t)$ as a function of frequency can be determined from the complex covariance S_{FG} defined as (Bendat & Piersol 1971)

$$S_{FG}(f) = C_{FG}(f) + iQ_{FG}(f), \tag{4.1}$$

where the real part $C_{FG}(f)$ is the frequency co-spectrum while the imaginary part Q_{FG} is the corresponding quadrature; the phase shift $\phi(f)$ is defined as

$$\phi(f) = \tan^{-1}\left\{\frac{Q_{FG}(f)}{C_{FG}(f)}\right\}. \tag{4.2}$$

As documented in Kumar *et al.* (2022), young random wind waves retain their coherency only over a duration that does not exceed a few dominant wave periods, whereas those computed from the experimental data values of the complex covariance $S_{\eta\eta_x(f)}$ are reliable only when both records are correlated reasonably well. To account for the fast loss of the temporal wave coherence, the phase shifts between η and η_x were calculated using (4.2) at each fetch x and wind velocity U only around the local $f_p(x)$ where the magnitude squared coherence values are sufficiently high, $M_{\eta\eta_x} = |S_{\eta\eta_x}|^2/(S_{\eta\eta}S_{\eta_x\eta_x}) > 0.8$. The resulting phase shifts $\phi(f)$ between η and η_x are plotted in figure 4(b). This phase shift ϕ for a linear unidirectional wave with amplitude a_0, $\eta(x, t) = a_0 \exp(i(k_x x - \omega t))$, is apparently $\pi/2$, whereas the measured phase shifts $\phi(f)$ in figure 4(b) remain systematically below this value, with the deviation of $\phi(f)$ from $\pi/2$ for all wind velocities U decreasing for longer waves with lower frequency f.
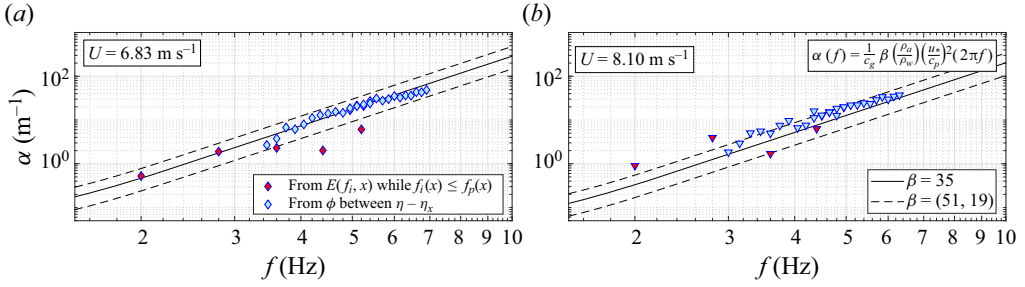
Figure 5. Variation of spatial energy growth rate, $\alpha(f)$, as a function of f at (a) $U = 6.83$ and (b) 8.10 m s^{-1}.

The assumption that the spatial inhomogeneity of the fetch-limited young wind waves is a result of the linear shear flow instability implies that the amplitude of each unstable harmonic varies with x, thus their wavenumbers are complex, $k_x(f) = k_{x,R}(f) + ik_{x,I}(f)$ (Zeisel *et al.* 2008). The dispersion relation defines the real part, Re($k_x(f)$), while the imaginary part, Im($k_x(f)$), represents the rate of the spatial variation of the wave amplitude (rather than energy as in (2.1)), thus $k_{x,I}(f) = i\alpha(f)/2$. Note that the relation $k_{x,R}(f)$, obtained in Geva & Shemer (2022a) from the solution of the coupled OS equations, agrees well with the empirical dispersion relations by Zavadsky *et al.* (2017) and Liberzon & Shemer (2011).

The surface elevation $\eta(x, t)$ and along-wind slope $\eta_x(x, t)$ therefore can be written as

$$\eta(x, t) = a_0 \exp(i(k_{x,R}x - \omega t)) \exp((\alpha/2)x), \qquad (4.3a)$$

$$\frac{\partial \eta(x, t)}{\partial x} = \eta_x(x, t) = (ik_{x,R} + \alpha/2)\eta(x, t). \qquad (4.3b)$$

The amplitude growth rate along the wave propagation direction is thus estimated as

$$\alpha(f)/2 = k_{x,R}(f) \tan\{\pi/2 - \phi(f)\} = \frac{k_{x,R}(f)}{\tan\{\phi(f)\}}. \qquad (4.4)$$

Equation (4.4) enables direct independent experimental estimates of the spatial energy growth rates $\alpha(f)$. The values of $\alpha(f)$ estimated using two independent methods for $U = 6.83$ and 8.10 m s^{-1} presented in figure 5 agree reasonably well. It should be emphasized that the growth rate estimates by both methods are only valid as long as the growth process is linear and thus the wave energy varies exponentially with fetch. This assumption can only remain valid for the harmonics below the peak frequency, see figure 3(a), which demonstrates that the evolution of the waves' energy at higher frequencies becomes strongly affected by nonlinear interactions, breaking, viscous dissipation, etc.

So far, the spatial growth rates α as a function of frequency f have been presented; however, to compare the present results with those available in the literature, the normalized temporal energy growth rates (γ/f) are now plotted as a function of inverse wave age (u_*/c), as done routinely to compile the data from various field and laboratory experiments, see Plant (1982). In order to enable consistent comparison with the results available elsewhere, the spatial growth rate values of $\alpha(f)$ measured here by two direct and independent methods are translated into temporal growth rates γ using the group velocity c_g that corresponds to the linear dispersion relation. The resulting values of γ/f obtained in the present study from the spatial variation of the energy of individual harmonics $E(f_i, x)$ for all $f < f_p(x)$ (red symbols), and from the single-point measurements of the phase difference $\phi(f)$ between $\eta - \eta_x$ (blue symbols), are plotted in figure 6 for different
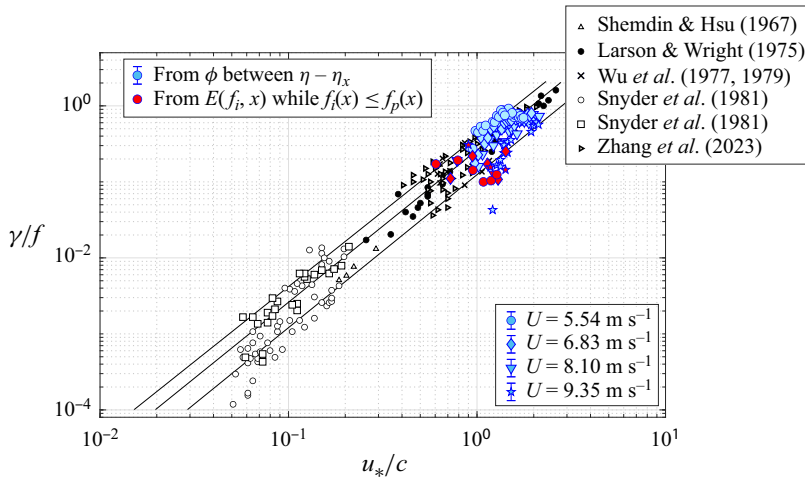
984 A22-10

Figure 6. Normalized temporal growth rate γ/f as a function of u_*/c. Black symbols are data compiled by Plant (1982); the solid lines represent fitting $\beta = 35 \pm 16$ in (1.1).

fetches and wind-forcing conditions. The data compiled by Plant (1982), as well as the recent results of Zhang *et al.* (2023), are also plotted in this figure.

The experimental results accumulated in the present study allow us to revisit the relation between the wave growth rate coefficient and the wave steepness suggested by Peirson & Garcia (2008). On the basis of diverse experimental data, they scaled the dependence of the dimensionless growth coefficient β in (1.1) on wave steepness ak as

$$\beta = 2\frac{(S_{in}/c)}{(\rho u_*^2)}\frac{1}{(ak)^2} = 2\frac{\tau_w}{\tau}\frac{1}{(ak)^2}, \tag{4.5}$$

where S_{in} is the total energy flux from air to water, c is the phase velocity, τ_w is the wave-coherent shear stress at the air–water interface and $\tau = \rho u_*^2$ is the total surface stress.

The spatial growth rate α derived here from measurement of the phase difference $\phi_{\eta,\eta_x}(f)$ enables us to plot in figure 7 the dependence of the growth rate coefficient β on the mean wave steepness $\overline{ak}$, directly estimated from the instantaneous slope records as $\overline{ak} = (\eta_{x,rms}^2 + \eta_{y,rms}^2)^{0.5} \approx \eta_{rms}k_p$ where $k_p = k(f_p)$. The error bar is the standard deviation in β representing the scatter in values estimated at each fetch for the frequency range where the cross-coherence coefficients exceed 0.8. The solid line $\beta = 2(ak)^{-2}$ in figure 7 corresponds to the case when the entire wave energy growth is associated with the wave-coherent shear stress. The values of the growth rate coefficient β in the present study agree well with the results of Mastenbroek *et al.* (1996), Grare *et al.* (2013) and Buckley *et al.* (2020). Note that, for the young wind waves studied here, the mean steepness $\overline{ak}$ is only dependent on the wind velocity U and remains quite high, mostly exceeding the value of $\overline{ak} = 0.15$ (Zavadsky & Shemer 2017*a*). Higher steepness is measured at the shortest fetch $x = 120$ cm where the wave field is still strongly affected by surface tension (Crapper 1984), while capillarity does not affect significantly longer waves at larger fetches. For those steep waves, the coefficients β obtained in the present measurements are close to the limiting value $2(ak)^{-2}$, thus the wave-related shear stress constitutes the major contribution to the total stress. This result is in agreement with Buckley *et al.* (2020), who observed in their experiments with mechanically generated waves that β approaches this limiting value with an increase in steepness.
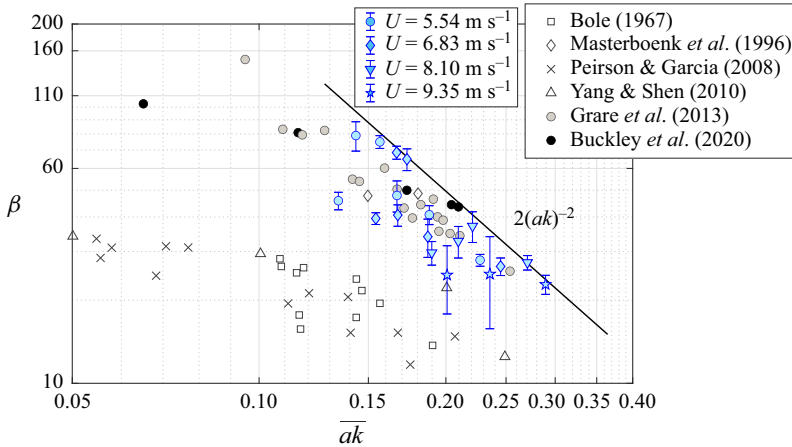
Figure 7. Wave growth coefficient β as a function of mean steepness $\overline{ak}$.

4.3. *Non-separated sheltering for young wind waves*

Variation of the energy of selected harmonics $E(f, x)$ presented in figure 3(*a*) demonstrates that their growth ceases to be governed mainly by linear shear instability for $f \geq f_p(x)$. For frequencies lower than $f_p(x)$, the energy influx S_{in} based on temporal growth rates presented in figure 6 enables evaluation at each fetch and wind velocity U of the effective non-separated sheltering coefficient s defined by Belcher & Hunt (1993) in terms of Jeffreys' sheltering hypothesis by the following equation:

$$\frac{S_{in}}{\omega E} = s \frac{\rho_a}{\rho_w} \left(\frac{U}{c} - 1 \right) \left| \frac{U}{c} - 1 \right|. \tag{4.6}$$

Here, s is the sheltering coefficient, U is the reference wind velocity given in table 1 and c is the wave propagation velocity at radian frequency ω. The energy influx S_{in} is evaluated using (4.5).

Following Peirson & Garcia (2008), the values of s are plotted in figure 8 as a function of mean wave steepness and are compared with additional available data (Bole & Hsu 1969; Mastenbroek *et al.* 1996; Peirson & Garcia 2008; Tan *et al.* 2023). The Plant relation (1.1) yields a constant value of $s = 0.05$ for $\beta = 35$. The values of the sheltering coefficient s in figure 8 are indeed scattered around this constant value and compare well with the results obtained in other studies. However, the decreasing trend with increasing steepness and wind velocity can be identified in figure 8 for steeper waves at high wind velocities (Buckley *et al.* 2020; Kumar *et al.* 2023; Tan *et al.* 2023) suggests decreasing the wave-coherent energy input S_{in}.

4.4. *Rates of the spatial evolution of wind waves at higher frequencies*

The presented results on the variation with fetch of the energy of each frequency harmonic $E(f, x)$ allow a closer look at their behaviour at fetches approaching and exceeding the location $x_p = x(f_p)$, where x_p is the fetch at which the frequency f corresponds to that of the spectral peak, see figure 2(*c*). At fetches around x_p, the transfer of energy and momentum is no longer governed mainly by exponential growth associated with linear shear flow instability; rather, it becomes affected by additional mechanisms such as nonlinear wave–wave interactions, sheltering and dissipation (Wu, Hsu & Street 1979).
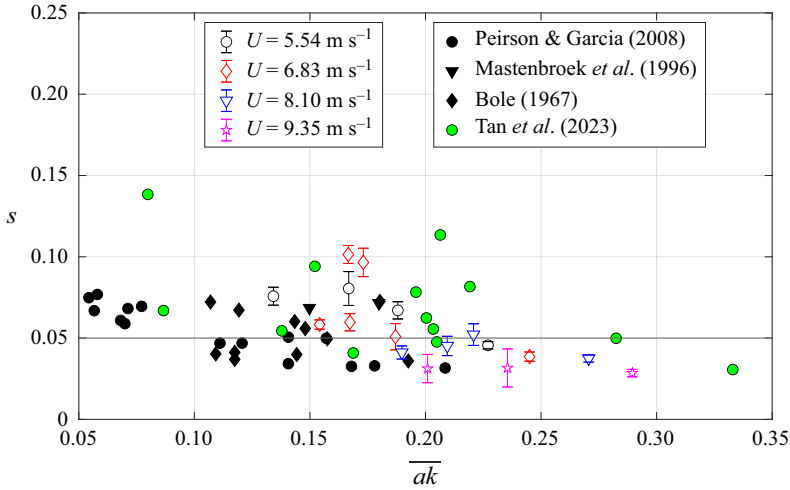
984 A22-12

Figure 8. Non-separated sheltering coefficient s as a function of mean steepness $\overline{ak}$. Black line: $s = 0.05$.
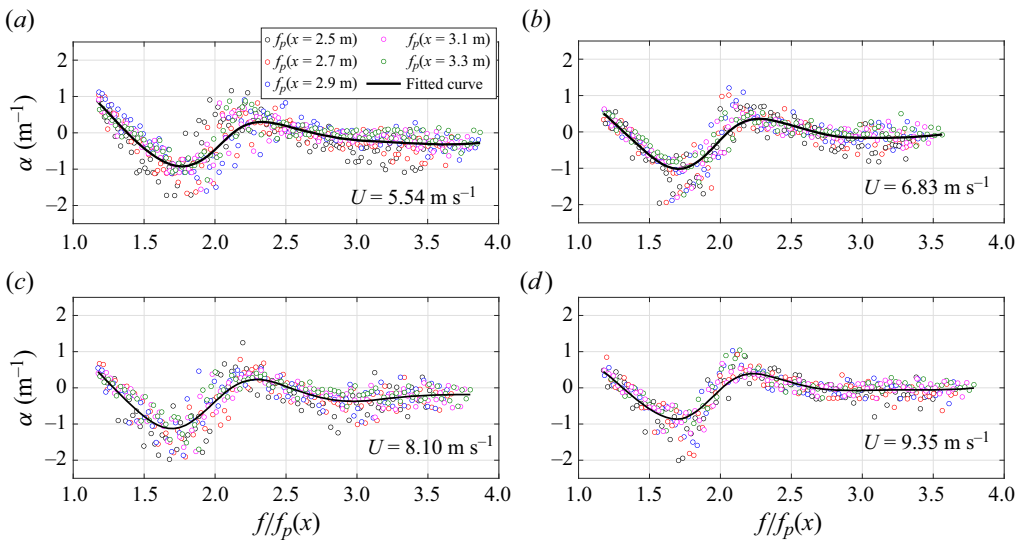

Figure 9. The effective spatial energy evolution rate $\alpha(f/f_p)$ in the frequency range $1.2f_p(x) \leq f < 4f_p(x)$. Smoothed mean values for each f/f_p are given by solid trend line.

For each harmonic f, the exponential fit is apparently inapplicable around fetches where it becomes the dominant one and attains its maximum amplitude. It is instructive, however, to analyse the spatial evolution of the energy of wave components with frequencies exceeding the local peak frequency $f > f_p(x)$ for $0 \leq x \leq x_p(f)$. Full sheltering of those components would result in zero or negative spatial evolution rates $\alpha(f)$.

Exponential fit of the variation of the spectral energy performed at those fetches allows determination of the corresponding effective values of $\alpha(f)$. Those results are plotted in figure 9 for all wind velocities and for several fetch-dependent peak frequencies in the range $1.2f_p(x) \leq f < 4f_p(x)$ as a function of $f/f_p(x)$. The solid lines clarify the characteristic trends of variation of $\alpha(f/f_p)$. The positive values of effective growth rate

984 A22-13

$\alpha(f/f_p)$ at frequencies slightly exceeding $f_p(x)$ can be attributed to the random character of wind waves. The instantaneously highest wave amplitude is not necessarily associated with the frequency f_p that represents the statistically significant value; frequencies in the vicinity of f_p may have instantaneously higher amplitudes, as can be seen in figure 1. This results in extension of the spatial domain where the energy of these waves increases due to shear flow instability.

The values of α in all panels of figure 9 become negative at approximately $f/f_p(x) = 1.3$ and continue to decrease monotonically up to approximately $f/f_p(x) \approx 1.7$. The decrease in values of $\alpha(f_i/f_p)$ is mostly associated with enhanced sheltering of the high-frequency wave component f_i by waves with higher amplitude downstream of $x(f_i)$, where the corresponding frequency harmonic attains its spectral peak value.

The decreasing trend in α ceases at $f/f_p > 1.7$ in all panels of figure 9; the variation rate then resumes its growth, becoming positive and attaining a local maximum f/f_p somewhat above 2. This energy growth can be attributed to the presence of second-order 'bound' waves that are prominent when the characteristic wave amplitudes around the spectral peak increase at higher fetches and wind velocities.

These bound waves of order $n = 2, 3, 4 \ldots$ with decreasing n amplitudes represent the generalization of higher-order contributions to the nonlinear monochromatic Stokes wave. They are routinely observed in experiments on mechanically generated regular or random steep waves with narrow spectrums. Any pair of waves with amplitudes a_i, a_j, both close to the peak frequency f_p, and frequencies f_i, f_j, make a second-order contribution to the spectrum at frequencies $(f_i + f_j)$, wavenumbers $(k(f_i) + k(f_j))$; the amplitudes of those waves are proportional to the product $a_i a_j$ (Stiassnie & Shemer 1987). All parameters of those bound waves, including their propagation velocities, are defined solely by their parent waves. The bound waves around the frequency $2f_p$ appear together with the 'parent' waves around the spectral peak frequency, as can be seen in 'clouds' associated with the second-order bound waves around the dashed line corresponding to $2f_p$ in figures 1(*a*)–1(*c*). Since the power spectra of wind waves are slightly positively skewed, as can be noticed in figure 2(*a*), the local peak in figure 9 is shifted to the right relative to $f/f_p = 2$. The impact of the second-order bound waves then gradually decreases; and spatial energy variation rates of harmonics at approximately $f/f_p > 2.5$, while exhibiting some scatter, become effectively negligible, suggesting the existence of nearly equilibrium conditions at those frequencies between wind input, dissipation and nonlinear effects.

5. Discussion

The empirical relation (1.1) with constant $\beta = 35 \pm 16$, suggested decades ago by Plant (1982), that was inspired by Miles (1957, 1960), based on diverse field and laboratory measurements, is still widely used to estimate the temporal growth rate of wind waves. However, Miles' non-viscous shear flow instability approach is monochromatic and deterministic, while wind waves are random and contain multiple harmonics, as shown e.g. in figure 1. Nevertheless, experiments by Larson & Wright (1975) and Plant & Wright (1977) demonstrated that, in a wind-wave field excited by impulsively applied wind, selected harmonics with fixed wavelengths in the gravity–capillary range indeed initially grow exponentially in time. Although the measured temporal growth rates differ significantly from the theoretical predictions, those experiments confirmed the applicability of the deterministic Miles inviscid shear flow instability approach to describe the initial growth in time of wind waves.

The experimental results presented by Kawai ([1976](#)) demonstrated exponential growth in time of the total energy of waves $\overline{\eta^2}$ excited by suddenly applied wind. In this study, Kawai also carried out computations using the viscous coupled OS equations, which demonstrated better agreement with experiments than that obtained in earlier attempts based on the inviscid Miles model. As stressed above, the theoretical models of shear flow instability of the duration-limited wind waves assume spatial homogeneity, whereas Larson & Wright ([1975](#)), Plant & Wright ([1977](#)) and, more recently and in greater detail, Zavadsky & Shemer ([2017*b*](#)), demonstrated that the impulsively excited young wind-wave field is much more complex; it approximately retains spatially homogeneity only for a limited duration which depends on fetch; during the subsequent evolution, the statistical wave parameters vary both in time and in space, before finally attaining the fetch-dependent and thus inhomogeneous quasi-steady state.

Since measuring wind waves under prescribed time-dependent forcing is virtually impossible in the field and is very complicated and demanding even in controlled laboratory conditions, the majority of experiments to validate the existing theories and models have been carried out for fetch-dependent wind waves excited by steadily blowing wind. To evaluate quantitatively the spatial evolution of a single harmonic in the frequency spectrum, some studies dealt with the spatial growth rate of a deterministic mechanically generated wave under steady forcing by carrying out measurements at multiple fetches (see Bole & Hsu ([1969](#)); Mitsuyasu & Honda ([1982](#)); Peirson & Garcia ([2008](#)) and Zhang *et al.* ([2023](#)) and references therein); attempts were made to compare the outcome with predictions of linear shear flow instability theories. Alternatively, sophisticated experimental and data processing methods were applied in single location measurements in which the variations with time of the surface elevation and of the normal and/or shear stresses, including the phase differences between them at the dominant frequency, were performed. Application of the momentum balance equation allows indirect estimates of temporal growth rates γ at that frequency (see Shemdin & Hsu ([1967](#)); Donelan *et al.* ([2006](#)); Donelan & Plant ([2009](#)); Liberzon & Shemer ([2011](#)) and Buckley & Veron ([2019](#)) and references therein). Paradoxically, those temporal growth rates are estimated in a wind-wave field that is statistically stationary, with the energies of each frequency harmonic remaining constant at the measuring location and varying with fetch only according to their spatial variation rates.

Unlike previous studies focused on a single harmonic, the present study deals with multiple frequency harmonics co-existing in the spectrum of young wind waves that are naturally excited by steadily blowing wind. To this end, extensive experiments were designed and carried out in our facility to enable direct estimates of the rates of the spatial variation of the amplitudes and energies at those frequencies by two direct and independent methods. The better understanding of mechanisms governing the variation with fetch of different frequency harmonics presented in § 4 opens a way to model and validate fetch-limited wind waves. An adequately modified to the spatial rather than temporal evolution case quasi-linear model based on the coupled OS equation can be used for this purpose. Such a model recently developed by Geva & Shemer ([2022*a*](#)) allowed quantitative modelling of evolving young wind waves under impulsive forcing. The initial growth of each harmonic in this model was attributed to linear viscous shear flow instability, with their harmonic growth rates obtained by solving coupled OS equations in air and water. An appropriate averaging procedure applied over the whole stochastic ensemble of multiple harmonics considered yielded a favourable comparison with the ensemble-averaged experimental results presented by Zavadsky & Shemer ([2017*b*](#)). To describe stages of wind-wave evolution that follow the initial linear stage with the exponential growth of

each harmonic, additional mechanisms such as breaking, sheltering, finite propagation duration and viscous dissipation were invoked. This treatment of the evolving wave field as an ensemble of multiple frequency harmonics, that resulted in favourable agreement with the experiments, indicated the importance of analysing numerous harmonics in the overall energy–momentum transfer.

Since the study of Gaster (1962), the temporal, γ, and the spatial, α, growth rates are customarily related using the wave group velocity. Zeisel *et al.* (2008) studied both temporal and spatial versions of the coupled OS equations and demonstrated that, in the framework of this linear viscous shear flow instability model, γ and α are indeed related by c_g. However, as pointed out in Shemer *et al.* (2020), the variation with frequency of the harmonics' group velocity $c_g(f)$ in a strongly dispersive gravity–capillary wind-wave field with finite spectral width may have a non-negligible effect on its spatial evolution. Moreover, it should be emphasized that the values of the temporal $\gamma(k)$ measured by Plant & Wright (1977) (in the duration-limited case), and of the spatial $\alpha(k)$ (in the fetch-limited case) growth rates for the same wavenumber k, are in fact not related exactly by the group velocity $c_g(k)$ calculated using the linear dispersion relation.

This discrepancy may be attributed to the fact that the eigenvalues of the OS equations that define the growth rates are dependent on the adopted velocity profiles in air and in water, especially near the critical layer in the air close to the air–water interface. The lin–log air velocity profile suggested for airflow over a smooth water surface by Miles (1960) has been adopted so far in all OS-based studies of viscous shear flow instability. Geva & Shemer (2022*a*) used this air velocity profile in their model for describing the evolution of waves excited by impulsively applied wind and obtained both quantitative and qualitative agreement with experiments. However, as mentioned above, in many experiments aimed at estimating the temporal wind-wave growth rate γ, measurements were performed under steady wind forcing blowing over spatially evolving waves. As evident from measurements by Zavadsky & Shemer (2012) and more recently by Geva & Shemer (2022*b*) and Kumar *et al.* (2023), the wave growth along the test section is accompanied by increasing with fetch effective surface roughness, resulting in significant deviation of the shape of the logarithmic velocity profile from that corresponding to the flow over a smooth surface. One can therefore expect that the temporal growth rates evaluated over rough wave surface may vary from those estimated for the duration-limited flow where the water surface is indeed initially smooth. Identification of a single frequency harmonic in a multicomponent random wind-wave field, as demonstrated in figure 1, is quite complicated. Nevertheless, understanding the mechanism governing the variation with fetch of each harmonic propagating over a rough surface is essential for quantitative comparison of predictions of wind-wave field evolution based on the coupled viscous OS shear flow instability model (Geva & Shemer 2022*a*) with measurements.

6. Conclusions

Two direct and independent methods were applied in our laboratory facility that allow measurement of spatial growth rates $\alpha(f)$ of young waves naturally excited by steadily blowing wind for a range of frequencies. In one series of experiments, simultaneous and synchronous measurements of $\eta(t)$ and $\eta_x(t)$ at a single point allowed evaluation of the phase difference ϕ_{η, η_x} between these two records for various wind velocities and fetches. The measured values of $\phi_{\eta, \eta_x}(f)$ for the spatially evolving wave harmonics are consistently below the phase difference $\phi_{\eta, \eta_x} = \pi/2$ for a linear homogeneous wave field. It is shown

that these measurements offer a novel way to evaluate directly the local spatial growth rate for a range of frequencies for which the records remain reasonably coherent.

In another set of experiments, measurements of power spectra $E(f)$ at densely spaced multiple locations along the tank were performed using conventional capacitance-type wave gauges. The obtained variation along the test section of the integral wind-wave field parameters such as the total energy $E_t(x) = \eta_{rms}^2(x)$ and the peak frequency $f_p(x)$ are found to follow the classical fetch-limited power relationships. However, the present detailed measurements along the test section allowed also the examination of the wave energy variation $E(f, x)$ with fetch for each harmonic separately. The results show that, at frequencies below the local peak frequency, $f < f_p(x)$, the wave energy of the naturally generated wind waves $E(f)$ grows exponentially with fetch x, thereby validating the assumption that linear shear flow instability serves as a primary growth mechanism. The spatial growth rates $\alpha(f)$ measured using this spectral approach for the selected frequency range agree well with the spatial growth rates derived independently from the measurements of the phase differences ϕ_{η,η_x}, as well as with diverse data available elsewhere and compiled by Plant (1982).

The wavelengths in the present experiments are sufficiently long for the spatial growth rate $\alpha(x)$ to decrease monotonically with wavelength $2\pi/k$ (Zeisel *et al.* 2008). Longer waves therefore grow slower and attain large amplitudes at larger distances; the dominant frequency $f_p(x)$ therefore decreases monotonically with fetch. This prompted a closer look at the behaviour of the spectral harmonics at higher frequencies beyond $f_p(x)$, which at remote fetches are partially sheltered by higher waves. The energy variation of those frequency harmonics at longer fetches ceases to be governed mainly by the linear shear flow instability. Additional physical effects become essential, such as sheltering by higher and longer waves, dissipation by various mechanisms and the effects of nonlinearity. Nevertheless, the experimental results indicate that the spatial evolution of harmonics with $f > f_p(x)$ can still be approximated by an exponential-in-x dependence with an effective spatial variation rate $\alpha(f)$. Since the local peak frequency $f_p(x)$ depends on fetch x and wind velocity U; it is advantageous to compare the effective wave energy variation rates α for those higher frequencies using the dimensionless frequency $f/f_p(x)$ as the horizontal axis. The present results clearly demonstrate that, for $f > f_p(x)$, the effective values of $\alpha(f)$ decrease initially and become negative due to sheltering by longer and higher waves. However, this decreasing trend is replaced by the increase in the apparent variation rate $\alpha(f)$ at frequencies in the vicinity of $2f_p(x)$. This increase is attributed to the contribution of the second-order bound waves. At frequencies significantly exceeding $2f_p(x)$, beyond the frequency domain of those bound waves, the measured evolution rates show some scatter but in general remain negligible, ostensibly cancelling the opposing effects on fetch evolution of wind input, dissipation and nonlinearity. The values of the effective spatial evolution rates $\alpha(f)$ obtained by an empirical fit for $f > f_p(x)$ reflect the combined effect of sheltering, dissipation and additional nonlinear mechanisms. Contrary to that, the exponential spatial wave energy growth with fetch at lower frequencies $f < f_p(x)$ is attributed to the linear viscous shear flow instability. The evolution with fetch of harmonics with frequencies below and above the local $f_p(x)$ is thus governed by essentially different physical mechanisms.

The results accumulated in the present study, in particular on the spatial growth rates $\alpha(f)$, were applied to compare the dependence on the mean steepness of the dimensionless growth rate coefficient β in (4.5). This comparison also allowed indirect estimation of the wind shear stress contribution to the wave growth. For mechanically generated small steepness waves, Buckley *et al.* (2020) found that only a certain portion of the total

shear stress acts towards the wave growth, while an increase in wave steepness leads to a higher contribution of the wave-coherent shear stress relative to the total. Our experiments are characterized by high steepness at all wind-forcing conditions and at all fetches. The dimensionless growth coefficients β presented in figure 7 thus correspond to those conditions and remain close to its limiting value for all wind-forcing conditions. This observation suggests that wave-coherent stress constitutes the dominant contribution to the total shear stress in young wind waves.

The experimental results were also analysed in terms of the non-separated sheltering hypothesis of Belcher & Hunt (1993). The energy influx estimated from phase difference measurement of η and η_x and (4.6) are used to estimate sheltering coefficients s that agree with results available elsewhere and are scattered about a constant value of $s = 0.05$. A decreasing trend in s is observed with an increase in steepness $\overline{ak}$ and wind velocity U, due to enhanced sheltering and a decrease in wind influx S_{in} for steeper and higher waves at higher wind velocity.

Finally, following Geva & Shemer (2022*a*), the present study emphasizes the co-existence of multiple harmonics in a wind-wave field and deals with each harmonic separately. The fundamentally random character of those waves, as demonstrated in figure 1, needs to be accounted for in any comparison of theoretical predictions based on deterministic shear flow instability theories with experimental results. A clear distinction is made between the fetch-limited and duration-limited cases. Fetch-limited waves excited by steady wind studied here are statistically stationary and grow as they propagate over the wavy water surface. Contrary to them, duration-limited waves are excited by impulsive forcing; they are assumed to be fetch-independent and grow in time over the initially smooth water surface. The fetch-limited and the duration-limited cases thus correspond to different effective roughnesses of the water surface and thus to different air velocity profiles. While it is generally accepted that the shape of the velocity profiles in air and in water affects shear flow instability, this issue has not yet been studied in depth. Nevertheless, the relation $\gamma(k) = c_g(k)\alpha(\omega)$ may not be applicable to the temporal growth rate $\gamma(k)$ of a wave excited by wind suddenly applied over a smooth water surface, and the spatial growth rate $\alpha(\omega)$ of a young wind wave with the same length that propagates over a wavy water surface with radian frequency $\omega = \omega(k)$. The large scatter in wind-wave growth rates presented in Plant (1982) that were acquired in diverse studies may be at least partially attributed to the very different physical conditions in those experiments.

Declaration of interests. The authors report no conflict of interest.

Author ORCIDs.
Lev Shemer https://orcid.org/0000-0003-0158-1823.

REFERENCES

BELCHER, S.E. & HUNT, J.C.R. 1993 Turbulent shear flow over slowly moving waves. *J. Fluid Mech.* **251**, 109–148.

BENDAT, J.S. & PIERSOL, A.G. 1971 *Random Data: Analysis and Measurement Procedure*. John Wiley and Sons.

BOLE, J.B. & HSU, E.Y. 1969 Response of gravity water waves to wind excitation. *J. Fluid Mech.* **35**, 657–675.

BUCKLEY, M.P. & VERON, F. 2019 The turbulent airflow over wind generated surface waves. *Eur. J. Mech. (B/Fluids)* **73**, 132–143.

BUCKLEY, M.P., VERON, F. & YOUSEFI, K. 2020 Surface viscous stress over wind-driven waves with intermittent airflow separation. *J. Fluid Mech.* **905**, A31.

CRAPPER, G.D. 1984 *Introduction to Water Waves*. John Wiley and Sons.

DONELAN, M.A., BABANIN, A.V., YOUNG, I.R. & BANNER, M.L. 2006 Wave-follower field measurements of the wind-input spectral function. Part II: parameterization of the wind input. *J. Phys. Oceanogr.* **36**, 1672–1689.

DONELAN, M.A. & PLANT, W.J. 2009 A threshold for wind-wave growth. *J. Geophys. Res.: Oceans* **114**, C07012.

GASTER, M. 1962 A note on the relation between temporally-increasing and spatially-increasing disturbances in hydrodynamic stability. *J. Fluid Mech.* **14**, 222–224.

GEVA, M. & SHEMER, L. 2022*a* A comprehensive approach to the problem of excitation of waves by wind: a theoretical model and experimental verification. *Phys. Rev. Lett.* **128**, 124501.

GEVA, M. & SHEMER, L. 2022*b* The wall similarity in turbulent boundary layers over wind-waves. *J. Fluid Mech.* **935**, A42.

GRARE, L., PEIRSON, W., BRANGER, H., WALKER, J., GIOVANANGELI, J. & MAKIN, V. 2013 Growth and dissipation of wind-forced, deep-water waves. *J. Fluid Mech.* **722**, 5–50.

HRISTOV, T.S., MILLER, S.D. & FRIEHE, C.A. 2003 Dynamical coupling of wind and ocean waves through wave-induced air flow. *Nature* **422**, 55–58.

JEFFREYS, H. 1925 On the formation of water waves by wind. *Proc. R. Soc. Lond.* A **107**, 189–206.

KAWAI, S. 1976 Generation of initial wavelets by instability of a coupled shear flow and their evolution to wind waves. *J. Fluid Mech.* **93**, 661–703.

KUMAR, K., GEVA, M. & SHEMER, L. 2023 Turbulent boundary layer profiles in airflow over young wind waves in co- and counter-wind water current. *Intl J. Heat Fluid Flow* **103**, 109210.

KUMAR, K., SINGH, S.K. & SHEMER, L. 2022 Directional characteristics of spatially evolving young waves under steady wind. *Phys. Rev. Fluids* **7**, 014801.

LARSON, T.R. & WRIGHT, J.W. 1975 Wind-generated gravity-capillary waves: laboratory measurements of temporal growth rates using microwave backscatter. *J. Fluid Mech.* **70**, 417–436.

LI, T. & SHEN, L. 2022 The principal stage in wind-wave generation. *J. Fluid Mech.* **934**, A41.

LIBERZON, D. & SHEMER, L. 2011 Experimental study of the initial stages of wind waves' spatial evolution. *J. Fluid Mech.* **681**, 462–498.

MASTENBROEK, C., MAKIN, V.K., GARAT, M.H. & GIOVANANGELI, J.P. 1996 Experimental evidence of the rapid distortion of turbulence in the air flow over water waves. *J. Fluid Mech.* **318**, 273–302.

MILES, J. 1957 On the generation of surface waves by shear flows. *J. Fluid Mech.* **3**, 185–204.

MILES, J. 1960 On the generation of surface waves by turbulent shear flows. *J. Fluid Mech.* **7** (3), 469–478.

MITSUYASU, H. 1970 On the growth of the spectrum of wind-generated waves. *Coast. Engng Japan* **13** (1), 1–14.

MITSUYASU, H. & HONDA, T. 1982 Wind-induced growth of water waves. *J. Fluid Mech.* **123**, 425–442.

MITSUYASU, H. & RIKIISHI, K. 1978 The growth of duration-limited wind waves. *J. Fluid Mech.* **85**, 705–730.

PEIRSON, W.L. & GARCIA, A.W. 2008 On the wind-induced growth of slow water waves of finite steepness. *J. Fluid Mech.* **608**, 243–274.

PHILLIPS, O.M. 1957 On the generation of waves by turbulent wind. *J. Fluid Mech.* **2**, 417–445.

PLANT, W.J. 1982 A relationship between wind stress and wave slope. *J. Geophys. Res.* **87**, 1961–1967.

PLANT, W.J. & WRIGHT, J.W. 1977 Growth and equilibrium of short gravity waves in a wind-wave tank. *J. Fluid Mech.* **82**, 767–793.

SHEMDIN, O.H. & HSU, E.Y. 1967 Direct measurement of aerodynamic pressure above a simple progressive gravity wave. *J. Fluid Mech.* **30**, 403–416.

SHEMER, L. 2019 On evolution of young wind-waves in time and space. *MDPI Atmos.* **10**, 562.

SHEMER, L. & SINGH, S. 2021 Spatially evolving regular water wave under the action of steady wind forcing. *Phys. Rev. Fluids* **6**, 034802.

SHEMER, L., SINGH, S. & CHERNYSHOVA, A. 2020 Spatial evolution of young wind waves: numerical modelling verified by experiments. *J. Fluid Mech.* **901**, A22.

STEWART, R.H & TEAGUE, C. 1980 Dekameter radar observations of ocean wave growth and decay. *J. Phys. Oceanogr.* **10**, 128–143.

STIASSNIE, M. & SHEMER, L. 1987 Energy computations for coupled evolution of class I and class II instabilities of stokes waves. *J. Fluid Mech.* **174**, 299–312.

SYNDER, R.L., DOBSON, F.W., ELLIOTT, J.A. & LONG, R.B. 1981 Array measurements of atmospheric pressure fluctuations above surface gravity waves. *J. Fluid Mech.* **102**, 1–59.

TAN, P., SMITH, A.W., CURCIC, M. & HAUS, B.K. 2023 Laboratory wave and stress measurements quantify the aerodynamic sheltering in extreme winds. *J. Geophys. Res.* **128**, e2022JC019505.

VALENZUELA, G.R. 1976 The growth of gravity-capillary waves in a coupled shear flow. *J. Fluid Mech.* **76**, 229–250.

WU, H.Y., HSU, E.Y. & STREET, R.L. 1979 Experimental study of nonlinear wave–wave interaction and white-cap dissipation of wind-generated waves. *Dyn. Atmos. Oceans* **3**, 55–78.

WU, J., POPINET, S. & DEIKE, L. 2022 Revisiting wind wave growth with fully coupled direct numerical simulations. *J. Fluid Mech.* **951**, A18.

YANG, D. & SHEN, L. 2010 Direct-simulation-based study of turbulent flow over various waving boundaries. *J. Fluid Mech.* **650**, 131–180.

ZAKHAROV, V.E., BADULIN, S.I., HWANG, P.A. & CAULLIEZ, G. 2015 Universality of sea wave growth and its physical roots. *J. Fluid Mech.* **780**, 503–535.

ZAVADSKY, A., BENETAZZO, A. & SHEMER, L. 2017 Study of spatial variability of short gravity waves in a wind wave tank by optical methods. *Phys. Fluids* **29**, 016601.

ZAVADSKY, A., LIBERZON, D. & SHEMER, L. 2013 Statistical analysis of the spatial evolution of the stationary wind-wave field. *J. Phys. Oceanogr.* **43**, 65–79.

ZAVADSKY, A. & SHEMER, L. 2012 Chracterization of turbulent airflow over evolving water-waves in a wind-wave tank. *J. Geophys. Res.* **117**, C00J19.

ZAVADSKY, A. & SHEMER, L. 2017a Investigation of statistical parameters of the evolving wind wave field using a laser slope gauge. *Phys. Fluids* **29**, 056602.

ZAVADSKY, A. & SHEMER, L. 2017b Water waves excited by impulsive wind forcing. *J. Fluid Mech.* **828**, 459–495.

ZAVADSKY, A. & SHEMER, L. 2018 Measurements of waves in a wind-wave tank under steady and time-varying wind forcing. *J. Vis. Exp.* **132**, e56480.

ZEISEL, A., STIASSNIE, M. & AGNON, Y. 2008 Viscous effects on wave generation by strong winds. *J. Fluid Mech.* **597**, 343–369.

ZHANG, J., HECTOR, A., RABAUD, M. & MOISY, F. 2023 Wind-wave growth over a viscous liquid. *Phys. Rev. Fluids* **8**, 104801.